

Inverse energy transfer in decaying, three dimensional, nonhelical magnetic turbulence due to magnetic reconnection

Pallavi Bhat^{1,2*}, Muni Zhou² and Nuno F. Loureiro²

¹ *Department of Applied Mathematics, University of Leeds, Leeds, LS2 9JT, UK*

² *Plasma Science and Fusion Center, Massachusetts Institute of Technology, Cambridge, MA 02139, USA*

16 July 2020

ABSTRACT

It has been recently shown numerically that there exists an inverse transfer of magnetic energy in decaying, nonhelical, magnetically dominated, magnetohydrodynamic turbulence in 3-dimensions (3D). We suggest that magnetic reconnection is the underlying physical mechanism responsible for this inverse transfer. In the two-dimensional (2D) case, the inverse transfer is easily inferred to be due to smaller magnetic islands merging to form larger ones via reconnection. We find that the scaling behaviour is similar between the 2D and the 3D cases, i.e., the magnetic energy evolves as t^{-1} , and the magnetic power spectrum follows a slope of k^{-2} . We show that on normalizing time by the magnetic reconnection timescale, the evolution curves of the magnetic field in systems with different Lundquist numbers collapse onto one another. Furthermore, transfer function plots show signatures of magnetic reconnection driving the inverse transfer. We also discuss the conserved quantities in the system and show that the behaviour of these quantities is similar between the 2D and 3D simulations, thus making the case that the dynamics in 3D could be approximately explained by what we understand in 2D. Lastly, we also conduct simulations where the magnetic field is subdominant to the flow. Here, too, we find an inverse transfer of magnetic energy in 3D. In these simulations, the magnetic energy evolves as $t^{-1.4}$ and, interestingly, a dynamo effect is observed.

Key words: (magnetohydrodynamics) MHD–turbulence–magnetic reconnection

1 INTRODUCTION

Turbulent processes are of fundamental importance to a wide range of systems, from quantum fluids to astrophysical plasmas (Skrbek & Sreenivasan 2012; Biskamp 2003). In a typical turbulent system, energy injected at a certain scale *direct* cascades down to smaller and smaller scales until it is dissipated by microphysical processes. On the other hand, an *inverse* cascade, or inverse transfer, involves energy being transferred from smaller to larger scales. This can occur in both forced or freely decaying turbulent systems (e.g., Davidson 2004). The best known inverse cascading system is two-dimensional (2D) hydrodynamic turbulence, where energy inverse cascades, while enstrophy direct cascades (Batchelor 1969; Kraichnan 1967). Indeed, the 2D hydrodynamic inverse cascade is widely considered one of the most important results in turbulence (Frisch 1995; Falkovich & Sreenivasan 2006) since Kolmogorov’s 1941 work. Both energy and enstrophy are inviscid invariants in 2D hydrodynamics. Here, the existence of more than one ideally conserved quadratic quantity in the system can lead to an inverse cascade (Nazarenko 2011). The 3D system mimics 2D-like inverse transfer when there is anisotropy due to strong rotation or the presence of a strong magnetic field (Yakhot & Pelz 1987; Baggaley

et al. 2014; Pouquet et al. 2019). Biferale et al. (2012) demonstrated that even in the case of 3D isotropic and homogeneous hydrodynamic turbulence, there can be an inverse cascade when parity (mirror symmetry) of the flow is broken.

Similarly, in 3D magnetohydrodynamics (MHD), it is well known that even in isotropic and homogenous decaying turbulence, inverse cascade occurs due to the presence of non-zero net magnetic helicity which breaks the parity in the system (Pouquet et al. 1976; Christensson et al. 2001). Magnetic helicity is a well-conserved quantity in the limit of large magnetic Reynolds number (R_m). Thus it is possible to have an inverse transfer in decaying turbulence in 3D MHD as long as it has helical magnetic fields (Christensson et al. 2001). However, recent simulations (Brandenburg et al. 2015; Zrake 2014; Berera & Linkmann 2014; Reppin & Banerjee 2017; Zhou et al. 2020) have shown that there exists an inverse transfer of magnetic energy in 3D MHD decaying turbulence, even in the absence of magnetic helicity.

In this paper we investigate the underlying cause of such a 3D nonhelical inverse transfer. We find that there are similarities between the 2D and 3D cases. The 2D inverse transfer has been previously well-studied and the ideal conserved quantities have been identified such as the total energy and vector-potential squared (Fyfe & Montgomery 1976; Pouquet 1978; Biskamp & Welter 1989). However, earlier 2D studies used Kolmogorov-type argu-

* P.Bhat@leeds.ac.uk

ments to obtain scaling solutions for the decaying field (Biskamp 2003). These arguments do not shine light upon the underlying physical processes responsible for the inverse transfer. In recent work by Zhou et al. (2019), a simple model based on merging magnetic islands provides a physical picture for the inverse transfer in the 2D system, and finds that the relevant timescale is that dictated by magnetic reconnection, which underlies such mergers. Here, we propose that magnetic reconnection is responsible for the 3D non-helical inverse transfer as well. Using direct numerical simulations, we study 3D, nonhelical, decaying MHD turbulence and build connections to the 2D case. We present evidence of similarities between 2D and 3D systems, and suggest magnetically dominated 3D systems display a 2D-like behavior.

We believe these findings are pertinent to several cosmological and astrophysical contexts. This reconnection-based understanding of the nonhelical inverse transfer, if true, affects the timescales of magnetic field evolution in the early universe (Banerjee & Jedamzik 2004; Sethi & Subramanian 2005; Subramanian 2016). Occurrence of reconnection in magnetically dominated decaying turbulence can be relevant to the understanding of high energy phenomena such as gamma-ray bursts and Crab nebula flares (Asano & Terasawa 2015; Zrake 2016; Blandford et al. 2017). Furthermore, such decaying turbulence has been studied in the context of star-formation in molecular clouds (Mac Low et al. 1998; Gao et al. 2015), and is relevant to the seeding of magnetic fields in protogalaxies from supernovae ejecta (Beck et al. 2013), and also in the case of galaxy-clusters after a merger event (Subramanian et al. 2006; Sur 2019). Zhou et al. (2020) present a discussion on the significance of inverse transfer in obtaining seed magnetic fields required for galactic dynamos (see their Appendix A).

2 NUMERICAL SETUP

2.1 The model

We use the PENCIL CODE¹ to simulate decaying MHD turbulence in both 2D and 3D. We solve the MHD equations given by

$$\frac{D \ln \rho}{Dt} = -\nabla \cdot \mathbf{u}, \quad (1)$$

$$\frac{D\mathbf{u}}{Dt} = -c_s^2 \nabla \ln \rho + \frac{\mathbf{J} \times \mathbf{B}}{\rho} + \frac{\mathbf{F}_{\text{visc}}}{\rho}, \quad (2)$$

$$\frac{\partial \mathbf{A}}{\partial t} = \mathbf{u} \times \mathbf{B} - \eta \mu_0 \mathbf{J}, \quad (3)$$

on a Cartesian N^2 or N^3 grid, with periodic boundary conditions, where N is the number of grid points in any given direction. The operator $D/Dt = \partial/\partial t + \mathbf{u} \cdot \nabla$ is the advective derivative, with \mathbf{u} the fluid velocity field. We solve the uncurled version of the induction equation, in terms of the vector potential, \mathbf{A} , related to the magnetic field by $\mathbf{B} = \nabla \times \mathbf{A}$. We adopt the Weyl gauge $\Phi = 0$, where Φ denotes the scalar potential. The current density is $\mathbf{J} = \nabla \times \mathbf{B}/\mu_0$, with μ_0 , the vacuum permeability. The viscous force is $\mathbf{F}_{\text{visc}} = \nabla \cdot 2\nu\rho\mathbf{S}$, where ν is the kinematic viscosity, and \mathbf{S} is the traceless rate of strain tensor with components $\mathbf{S}_{ij} = \frac{1}{2}(u_{i,j} + u_{j,i}) - \frac{1}{3}\delta_{ij}\nabla \cdot \mathbf{u}$ (commas denote partial derivatives). Finally, η is the magnetic diffusivity. In the 2D

Table 1. A summary of all runs and their respective parameters (in dimensionless units). u_{rms0} and B_{rms0} are the initial root-mean-squared values of the flow and the magnetic field respectively. In all runs the initial $k_p \approx 25$.

Run	Resolution	$\eta \times 10^4$	u_{rms0}	B_{rms0}	S
A2D	2048 ²	0.5	0.0	0.2	1000
B2D	1024 ²	1.0	0.0	0.2	500
C2D	1024 ²	2.0	0.0	0.2	250
F2D	1024 ²	1.0	0.2	0.02	50
A3D	1024 ³	0.5	0.0	0.2	1000
B3D	1024 ³	1.0	0.0	0.2	500
C3D	512 ³	2.0	0.0	0.2	250
D3D	512 ³	4.0	0.0	0.2	125
E3D	512 ³	8.0	0.0	0.2	50
F3D	1024 ³	0.25	0.2	0.02	200

runs, we solve a 2D version of equations (1 - 3) obtained by setting $\partial_z = 0$ and eliminating vector components in the z direction. Other than compressibility effects (which are minor in our simulations), this 2D version of the equations is identical to the 2D version of the reduced-MHD equations Kadomtsev & Pogutse (1974); Strauss (1976); Schekochihin et al. (2009). The code uses dimensionless quantities by measuring length in units of the domain size L , speed in units of the isothermal sound speed c_s , density in units of the initial value ρ_0 and magnetic field in units of $(\mu_0\rho_0c_s^2)^{1/2}$. We choose $L = 2\pi$, and $c_s = \rho_0 = \mu_0 = 1$.

2.2 Initial conditions and parameters

The initial magnetic field is generated in the wavenumber space with a certain spectrum and random phases, similar to the method in Brandenburg et al. (2015). The magnetic power spectrum is k^4 (Brandenburg et al. 2015) for $k < k_0$, and is exponentially cutoff beyond k_0 . Such a spectrum is obtained from the vector potential in Fourier space, $\hat{A}_j(\mathbf{k})$, whose three components j are given by,

$$\hat{A}_j(\mathbf{k}) = A_0(k^2/k_0^2)^{n/4-1/2} \exp(-k^2/k_0^2) \exp(i\phi(\mathbf{k})) \quad (4)$$

where exponent $n = 2$, $\phi(\mathbf{k})$ are random phases and A_0 is the amplitude.

We define the Lundquist number in our simulations as $S = V_A(2\pi/k_p)/\eta$, where V_A is the Alfvén velocity and k_p is the wavenumber at which the magnetic power spectrum peaks. In our main runs, the initial Alfvén velocity is $V_A = 0.2$ (which implies that compressibility effects are weak and can be ignored in the analysis of the dynamics) and the initial velocity field is zero, analysed in sections 3.1-3.3. We have also carried out runs with non-zero initial velocity field; these are reported in section 3.4. In all runs, initial $k_p \approx 25$. We have run simulations across a range of Lundquist numbers as allowed by the resolution limit of 2048² in 2D and 1024³ in 3D. The magnetic Prandtl number in all our simulations is 1. A list of all runs reported in this paper is shown in Table 1.

3 RESULTS

3.1 Decaying turbulent magnetic fields in 2D

We first present our study of 2D simulations of decaying MHD turbulence (simulations A2D, B2D and C2D in Table 1). In the top

¹ DOI:10.5281/zenodo.2315093, github.com/pencil-code

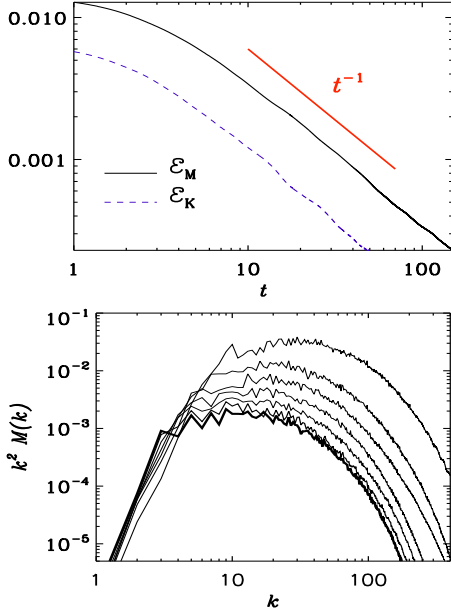


Figure 1. Top panel: Evolution of magnetic energy (solid black) and kinetic energy (dashed blue) in a 2D simulation, A2D, with $S = 1000$ and resolution of 2048^2 . Bottom panel: Compensated magnetic power spectra $k^2 M(k, t)$ are plotted at regular intervals of $\Delta t = 10$ with a thick final curve at $t = 70$.

panel of Fig. 1, the evolution of magnetic energy is shown in a log-log plot. It decays in time as a power law, with an exponent close to -1 at late times. This result matches with that obtained in the 2D simulations performed by Zhou et al. (2019), which focused on an initial condition consisting of an ordered array of current filaments (or, equivalently, magnetic islands) with alternating polarities. Upon introducing small perturbations into that system, the current filaments move out of the initial (unstable) equilibrium. The subsequent evolution of the system is then primarily dictated by the coalescence, via magnetic reconnection, of filaments with equal polarity. Mergers of island pairs lead to larger islands, albeit at the cost of magnetic energy dissipation. Successive mergers lead to progressively larger structures, resulting in an inverse transfer of magnetic energy. This occurs hierarchically in a self-similar manner, giving rise to power-law-in-time behaviour. Similarly, even in the case of a random initial condition such as employed here, we observe an inverse transfer as the system evolves in time. This is quite evident in the time progression of the magnetic power spectrum, shown in the bottom panel of Fig. 1. The initial spectrum (random field peaked at $k_p \sim 25$) is seen to shift from large wavenumbers to smaller ones, depicting an inverse transfer. The spectra are compensated by k^2 to reveal a range where they flatten; the same power law is observed by (Zhou et al. 2019), who attribute it to the dominance of sharp current sheets. (i.e., a Burgers’ spectrum (Burgers 1948)).

As in Zhou et al. (2019), the growth of magnetic energy at large scales that we find in our 2D simulations is due to magnetic reconnection. This can be seen explicitly and clearly from a sequence (a movie) of time evolving contour plots of A_z (see supplementary material), or from the corresponding stills at specific moments of time shown in Fig. 2. Current sheets — sharply localized enhancements of current density in Fig. 3 — are seen to form at the interface of any pair of interacting islands, leading to their reconnection and resulting in larger islands. The magnetic islands can be seen to grow progressively larger in time due to island mergers.

A complementary way to understand inverse transfer in this 2D system is to consider the conserved quantities in the system. For the ideal 2D MHD equations (in the absence of dissipation), these are the total energy, $\mathcal{E}_M + \mathcal{E}_K = \langle \mathbf{B}^2 \rangle / 2 + \rho \langle \mathbf{u}^2 \rangle / 2$ (given weak compressibility), and vector-potential squared, $P = \langle \mathbf{A}^2 \rangle$, (where $\langle \rangle$ represents integral over the domain) (e.g., Biskamp 2003). In the following we show that in our non-ideal system where the kinetic energy is subdominant, by considering the evolution of \mathcal{E}_M and P , we can deduce that decaying 2D MHD turbulence displays inverse transfer of energy. The evolution equations for magnetic energy and vector-potential squared in a closed domain (given periodic boundaries in the DNS) in the non-ideal case are given by,

$$\iint dS \frac{\partial}{\partial t} \left(\frac{\mathbf{B}^2}{2} \right) = - \iint dS \mathbf{u} \cdot (\mathbf{J} \times \mathbf{B}) + \eta \mathbf{J}^2, \quad (5)$$

$$\iint dS \frac{D}{Dt} \left(\frac{A_z^2}{2} \right) = - \iint dS \eta \mathbf{B}^2. \quad (6)$$

In the 2D limit that we consider here, only one component of the vector potential is needed, i.e. $\mathbf{B} = \nabla \times A_z \hat{z}$, where the \hat{z} is the unit vector orthogonal to the 2D plane. Similarly, only one component of the current density survives, $J_z = \partial_x B_y - \partial_y B_x$.

From Eqs. (5) and (6), it is possible to deduce the following implications for a freely evolving turbulent system. While the evolution of vector potential squared is governed by only a decay term on the RHS of Eq. (6), the equation for magnetic energy, Eq. (5), also consists of a source term given by $\mathbf{u} \cdot (\mathbf{J} \times \mathbf{B})$. Depending on the sign of this term, either the energy is being transferred from the magnetic field to the velocity field, or *vice versa*. Now, in these simulations, the velocity field is initially zero, and it is entirely driven by the magnetic field. We assume that the back-reaction from the generated flow on the field is negligible: this is a reasonable assumption if the kinetic energy is subdominant, as is indeed the case in our system (see the top panel of Fig. 1). Thus, as the system is allowed to evolve freely, the magnetic field loses its energy to either the velocity field or to resistive decay. Given that the system is turbulent, the magnetic field is expected to decay even as $\eta \rightarrow 0$ because the field can develop small enough scales (current sheets). As a result, $\eta \langle \mathbf{J}^2 \rangle$ can remain finite in that limit. However, as $\eta \rightarrow 0$, the term on the right hand side of Eq. (6), $\eta \langle \mathbf{B}^2 \rangle$ (where $\langle \mathbf{B}^2 \rangle$ is essentially independent of resistivity) will go to zero, thereby rendering volume-integrated vector-potential squared, P , to be nearly invariant. In short, in the limit of $\eta \rightarrow 0$ (or, equivalently, in the limit of very large R_m or S), the vector potential squared is better conserved than the magnetic energy, $\mathcal{E}_M = \langle \mathbf{B}^2 \rangle / 2$.

We can now use this conservation property to argue why such a freely decaying turbulent system can exhibit inverse transfer. In the Fourier domain we have $\hat{\mathbf{B}} = i\mathbf{k} \times \hat{A} \hat{z}$, where $\mathbf{k} = k_x \hat{x} + k_y \hat{y}$. It follows that

$$|\hat{\mathbf{B}}|^2 = k^2 |\hat{A}|^2. \quad (7)$$

Now, let us use the expressions for \mathcal{E}_M and P in the Fourier domain,

$$\mathcal{E}_M = \frac{1}{2} \int |\hat{\mathbf{B}}|^2 d^2 \mathbf{k}, \quad (8)$$

$$P = \int |\hat{A}|^2 d^2 \mathbf{k}, \quad (9)$$

and consider that most of the magnetic energy is concentrated in a single scale in the system; we shall call it the correlation scale, k_{corr} . It then follows from Eq. (7) that

$$k_{\text{corr}} \sim \sqrt{\mathcal{E}_M / P}. \quad (10)$$

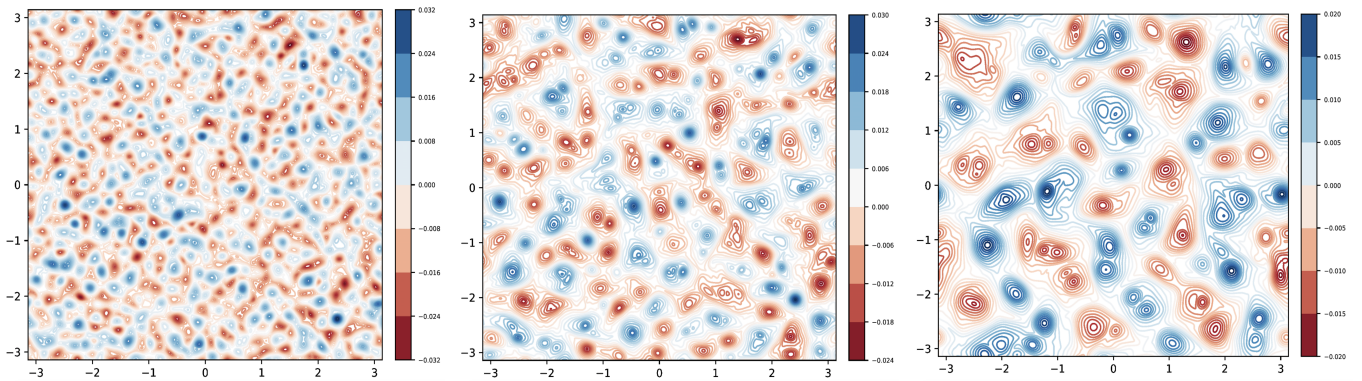


Figure 2. Evolution of the vector potential (A_z) in the 2D simulation A2D, with $S = 1000$. The times plotted are $t = 1$, $t = 15$ and $t = 45$, from left to right.

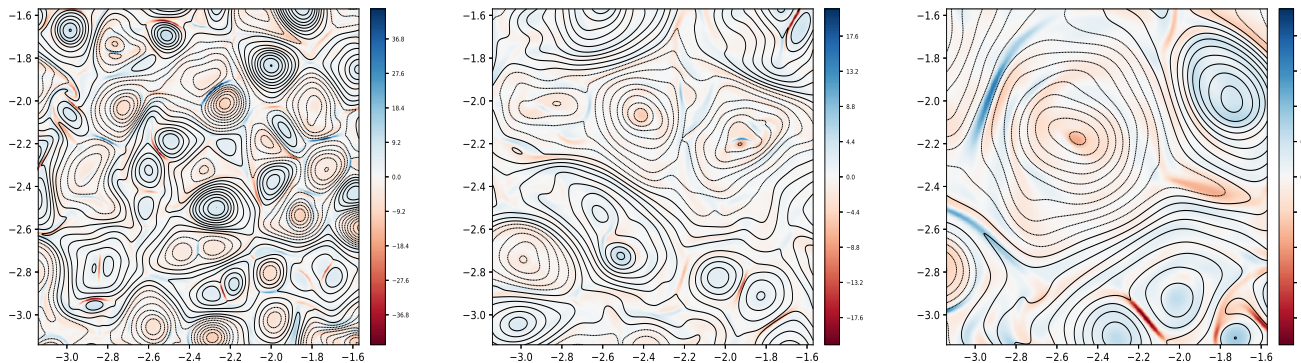


Figure 3. Evolution of the current density (J_z) in $1/8$ of the domain from the 2D simulation A2D, at times $t = 1$, $t = 15$ and $t = 45$, from left to right. The overlaid lines are contours of A_z .

Since this is an unforced stochastic system, the magnetic energy, \mathcal{E}_M , will decay. Given that P is better conserved than \mathcal{E}_M , P remains nearly constant as \mathcal{E}_M decreases; thus, the wavenumber k_{corr} is expected to decrease. This implies a shift of the correlation scale in the system to larger and larger scales — the spectral signature of an inverse transfer. Indeed, if we substitute the scaling $\mathcal{E}_M \propto t^{-1}$ into Eq. (10), and consider P to be constant in time, we obtain $k_{\text{corr}} \propto t^{-1/2}$. This is consistent with what we find from our simulations when we trace k_{corr} as a function of time. Both of these scalings are predicted by the reconnection-based hierarchical model of Zhou et al. (2019), and are verified by the RMHD numerical simulations carried out in that paper (note that the hierarchical model itself is based on mass and magnetic flux (A_z) being conserved during island mergers through reconnection). Thus, we conclude that the implications from 2D conservation properties are consistent with the physical picture of island mergers via reconnection in 2D; together, they provide a solid explanation for the inverse transfer of magnetic energy in the 2D system.

3.2 Decaying turbulent nonhelical magnetic fields in 3D

Next, we turn to 3D simulations (runs A3D, B3D, C3D, D3D and E3D in Table 1). The 3D run resolutions go up to 1024^3 grid points, and all have an initial condition similar to the 2D case of random

magnetic fields with power peaked at small scales, as specified in Eq. (4).

As in the 2D case, we again observe a power-law-in-time magnetic energy decay with exponent -1 , as shown in the top panel of Fig. 4 (at later times, the decay of magnetic energy steepens, possibly due to diffusion beginning to dominate the system. Brandenburg et al. (2015), who use a similar setup, do not report such a transition, possibly because the higher resolution that they employ (2304^3) reduces diffusive effects in their simulation).

From the bottom panel of Fig. 4, a flat range indicating k^{-2} slope in the magnetic spectrum can be observed (Brandenburg et al. 2015; Zrake 2014), however with limited range given the resolution. These scalings are intriguingly similar to the ones seen already in the 2D case, thus triggering the following questions:

- (i) To what extent are the 3D simulations similar to the 2D ones?
- (ii) Can we conclude that, even in 3D, "structure mergers" via reconnection are responsible for this inverse transfer of magnetic energy?

This section and the next are concerned with answering these questions.

Firstly, we see in Fig. 5 qualitative similarities with the 2D runs; namely, the evolution of the magnetic field structures (from a slice out of the 3D domain) resembles the behaviour of the magnetic islands seen in the contour plots from the 2D system (Fig. 2).

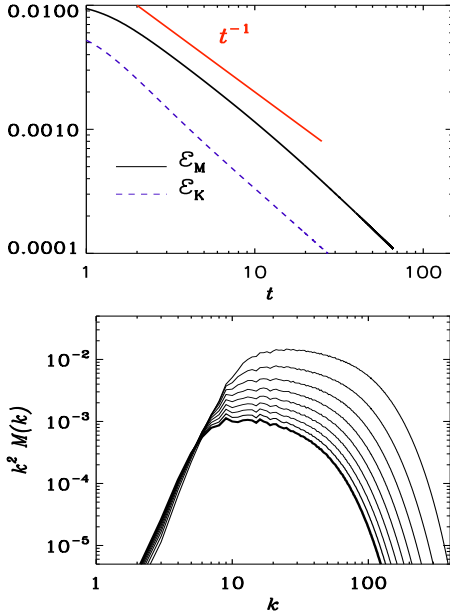


Figure 4. Top panel: evolution of magnetic energy (solid black) and kinetic energy (dashed blue) in the 3D simulation A3D, with $S = 1000$ and resolution of 1024^3 . The bottom panel shows compensated magnetic power spectra $k^2 M(k, t)$ for the same run, plotted at regular intervals of $\Delta t = 5$, with a thick final curve at $t = 50$.

We also show the evolution of the x -component of the field, B_x , in Fig. 6. It is clearly seen that the field structures grow in scale. However, here in the 3D case, the structures are more elongated and are not as symmetric as in the 2D case. Nonetheless, they do not exhibit any specific directionality overall. In other words, while locally each field structure does seem to prefer a certain direction (given the elongation), these preferences are randomly distributed over the domain. Thus, there is no development of a large-scale structure which can bias the system in a certain randomly chosen direction, as is routinely seen, for example, in helical dynamos (Brandenburg & Subramanian 2005).

From comparisons with the 2D results, there is a suggestion that perhaps, even in the 3D system, a reconnection-based mechanism might be responsible for the growth of the structures over time (Zhou et al. (2020) have explored the suggestion in this work, also in the context of reduced-MHD, and found it to correctly describe their numerical results). To further support this suggestion, we show in Fig. 7 the absolute value of the current density, $|\mathbf{J}| = \sqrt{J_x^2 + J_y^2 + J_z^2}$. The wispiqueness of the current density structures corroborates the existence of current sheets where reconnection can take place.

Already at this point it is possible to argue for why there are similarities between the 2D and the 3D results. Given that the system is magnetically dominated, we think that strong local anisotropy spontaneously arises. This is reflected in the previously mentioned elongation of the magnetic structures in Figs. 5 and 6. This local anisotropy, then, could lead to 2D-like behaviour. While the Sweet-Parker scaling of magnetic reconnection rate does not change from 2D to 3D, this local anisotropy entails the possibility of the existence of local guide-fields, if required to render the 3D reconnections with 2D-like behaviour. This would explain why we see results in 3D which are similar to that in 2D (such as the magnetic energy scaling of t^{-1} and the spectral scaling of k^{-2}).

Next, we look at the conservation properties in both the 2D

and 3D systems. First, we show in the top panel of Fig. 8 the evolution of the rate of change of the 2D MHD ideal invariants P (black) and \mathcal{E}_M (red-dashed) (given that kinetic energy is subdominant here), $\lambda_A = d(\ln P)/dt$ and $\lambda_B = d(\ln \mathcal{E}_M)/dt$, respectively, calculated from run A2D. As expected, λ_A is much smaller than λ_B , thus demonstrating P to be better conserved than \mathcal{E}_M , as we have argued earlier. In the bottom panel of Fig. 8, we show the evolution of λ_A and λ_B from the 3D simulation A3D, and again we find the former to be much smaller than the latter. While theoretically P is strictly an ideal invariant only in 2D, these results suggest that it is possible to make a case for its approximate conservation in 3D as well.

Consider, therefore, the evolution of P in 3D,

$$\int dV \frac{D}{Dt} \left(\frac{\mathbf{A}^2}{2} \right) = \int dV \mathbf{u} \cdot (\mathbf{A} \cdot \nabla \mathbf{A}) - \eta \mathbf{B}^2. \quad (11)$$

This equation differs from the 2D case only by the term $\mathbf{u} \cdot (\mathbf{A} \cdot \nabla \mathbf{A})$ on the RHS. Here, again, we appeal to the fact that flow is subdominant to the field in order to assume that backreaction of the flow on the field is negligible. Such subdominance can be seen in Fig. 9: in the vicinity of the peak wavenumber, the amplitude of the kinetic power spectra are lower than the magnetic power spectra by about an order of magnitude, in both 2D and 3D cases. Furthermore, the source term $\mathbf{u} \cdot (\mathbf{A} \cdot \nabla \mathbf{A})$ in question from Eq. (11) can be compared to the analogous source term in the equation for the magnetic energy Eq. (5), $\mathbf{u} \cdot (\mathbf{B} \cdot \nabla \mathbf{B})$ (Note that Eq. (5) is valid in 3D also). This term arises on expanding $\mathbf{u} \cdot (\mathbf{J} \times \mathbf{B}) = \mathbf{u} \cdot (-\nabla(\mathbf{B}^2/2) + \mathbf{B} \cdot \nabla \mathbf{B})$. Assuming that $|\mathbf{B}| \sim k_{\text{corr}} |\mathbf{A}|$ (in a scenario where most of the power is in a single scale, represented by the wavenumber $k_{\text{corr}} \gg 1$), then these sources differ by a factor of k_{corr}^2 , with the term $\mathbf{u} \cdot (\mathbf{A} \cdot \nabla \mathbf{A})$ being smaller of the two. Thus, again, we conclude that in the limit of $\eta \rightarrow 0$, P decays much slower than \mathcal{E}_M . Consequently, it follows from Eq. (10) that there can be an inverse transfer in 3D as well, as seen in the 3D simulations.

Since we are dealing with quantities based on vector potential, a fair concern is with regard to the gauge dependence. As mentioned earlier, our model equations adopt the Weyl gauge ($\Phi = 0$). To check for possible gauge-related effects in the results, we performed a simulation using instead the Lorenz gauge, with the same parameters and initial conditions as those employed in our main runs with the Weyl Gauge. In the Lorenz gauge (or the pseudo-Lorenz gauge), we have $\partial_t \Phi = -c_s^2 \nabla \cdot \mathbf{A}$ (Brandenburg & Käpylä 2007), where c_s is the speed of sound instead of the speed of light. We overplot the result in the bottom panel of Fig. 8 (dotted blue line). It can be seen that the results from the Lorenz gauge are indistinguishable from those with the Weyl gauge. This is consistent with the expectation of better conservation of P than of \mathcal{E}_M to hold up in any gauge within a closed domain, as the sink terms in the equations for P and \mathcal{E}_M remain the same.

While these arguments based on ideal conserved quantities are useful to provide plausibility to the notion that the understanding of 3D nonhelical inverse transfer lies in its 2D like behaviour, we still do not have more substantial evidence for reconnection being the driving factor for the inverse transfer. To gain a better understanding of the system, we study the timescale governing its dynamical evolution. In doing so, we continue to probe the similarities between the 2D and 3D cases.

The power law governing the evolution of the magnetic field in the 2D system is expected to be $B_{\text{rms}} = B_0 (t/\tau_{\text{rec}})^{-1/2}$ as shown by Zhou et al. (2019), where τ_{rec} is the reconnection time scale, given by $\tau_{\text{rec}} = \beta_{\text{rec}}^{-1} (2\pi/k_{\text{corr}0})/V_{A0}$, with β_{rec} the normalized

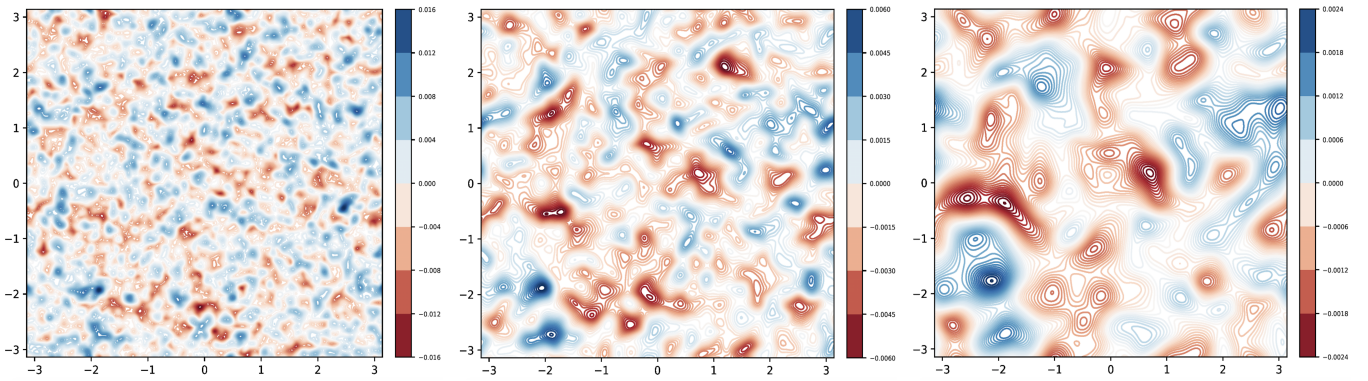


Figure 5. Contour plots of the z -component of the vector potential (A_z), in an arbitrary 2D slice (in the $x - y$ plane) from the 3D simulation C3D. The times plotted are $t = 2$, $t = 15$ and $t = 50$, from left to right.

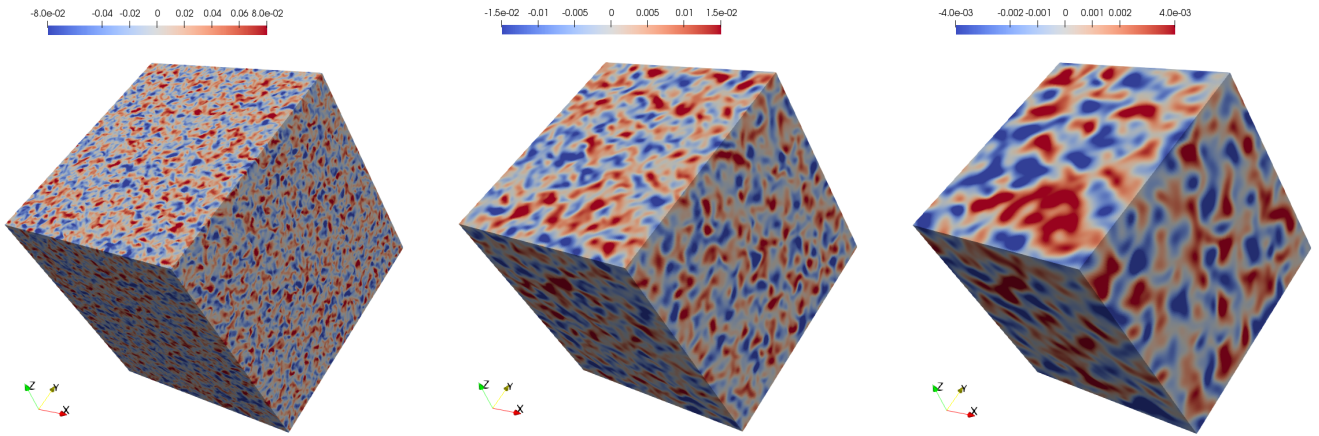


Figure 6. Evolution of a component of the magnetic field, B_x , shown on the 3D domain from the 3D simulation, C3D, at times $t = 2$, $t = 15$ and $t = 50$ from left to right.

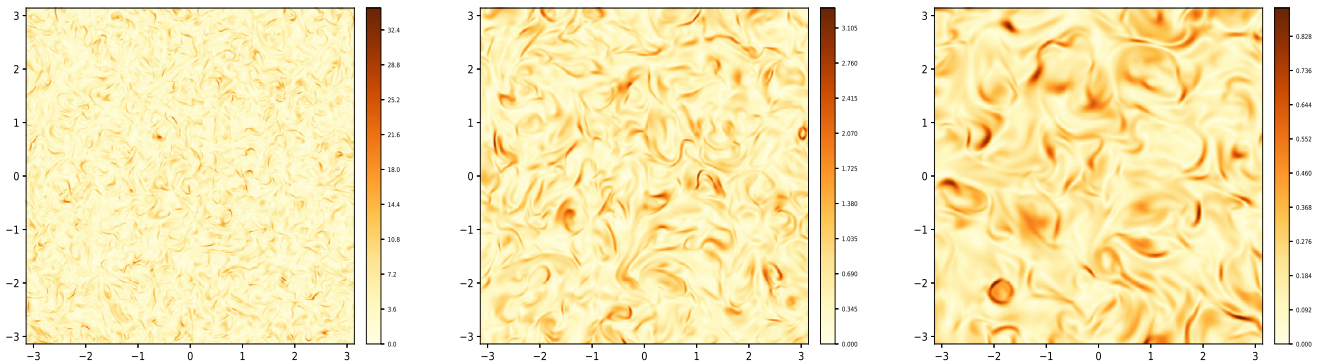


Figure 7. Evolution of the absolute value of the current density ($|J|$) in 1/4 of the domain of an arbitrary 2D slice from the 3D simulation, A3D, shown in contour plots at times $t = 3$, $t = 21$ and $t = 60$, from left to right.

reconnection rate, $k_{\text{corr}0}$ is the wavenumber associated with the initial correlation scale and V_{A0} is the initial Alfvén velocity. Here we use the Sweet-Parker scaling for the reconnection rate Sweet (1958); Parker (1957), $\beta_{\text{rec}} = S^{-1/2}$, which is appropriate for values of S lower than the value critical to trigger the plasmoid

instability (Loureiro et al. 2007; Samtaney et al. 2009). Note that as the simulation proceeds, the correlation scale, $(2\pi/k_{\text{corr}})$ (we take $k_{\text{corr}} = k_p$) increases and the Alfvén velocity, V_A , decreases, and thus the Lundquist number, $S = V_A(2\pi/k_{\text{corr}})/\eta$ is expected to remain constant (Zhou et al. 2019). For two different runs with

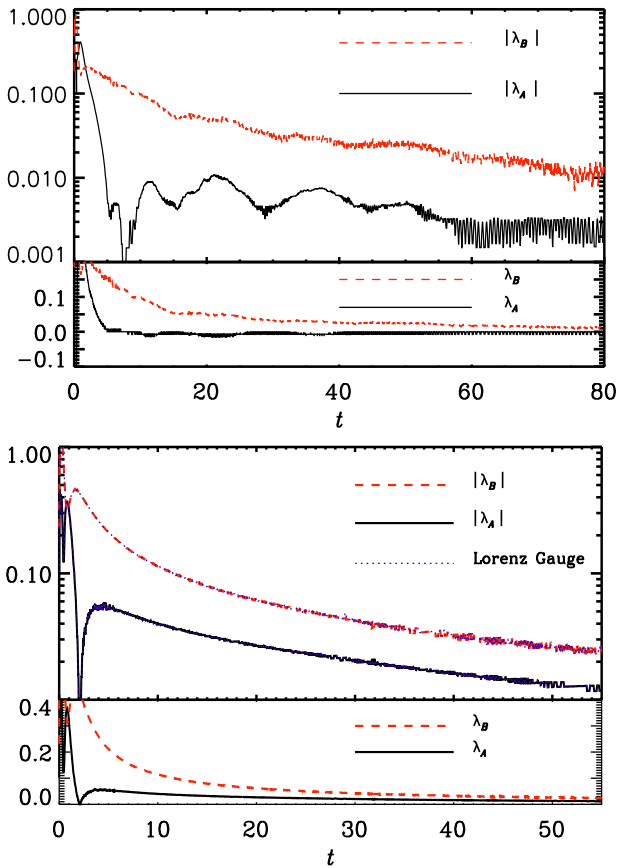


Figure 8. The rate of change of vector potential squared, λ_A (dashed red), and magnetic energy, λ_B (solid black), is shown for 2D and 3D simulations, A2D and A3D (where $S = 1000$) in the top and bottom figures, respectively. In each figure, the upper panel is a log-linear plot, whereas the lower panel is a linear-linear one. In the bottom figure, an additional panel curve from a 3D simulation employing the Lorenz gauge is shown in dotted blue.

different Lundquist numbers S_1 and S_2 , at any given time t , the ratio of the magnetic field strengths is then predicted to scale as $B_{\text{rms}1}/B_{\text{rms}2} = (S_1/S_2)^{1/4}$.

In Figs. 10 and 11, we compare B_{rms} evolution curves from 2D and 3D runs, respectively, with different values of S , which vary by a factor of 2 from one run to another. In the bottom panels of Figs. 10 and 11, we normalize the time axis by the reconnection timescale τ_{rec} (note that the normalization τ_{rec} is computed for the initial k_{corr} and not varied with time; this is because k_{corr} is a discrete quantity and thus its variation does not lead to a secular evolution of the time axis t/τ_{rec}). On applying this normalization, there is a notable tendency for curves from different simulations to collapse on top of each other. The collapse of the curves is better in the 2D case than the 3D case; but, even in the 3D case, for runs with increasing values of S , the gap between the successive curves decreases. The curves from runs with the highest resolution and Lundquist numbers, $S = 500$, shown in dash-dotted green, and $S = 1000$, shown in dotted black, very nearly collapse on top of each other. These results suggest that the reconnection timescale dictates the dynamical evolution of both the 2D and the 3D systems. A point to be noted is that when the time axes are normalized by the resistive timescale instead, the curves do not collapse together.

This result of curves collapsing together on normalization of time by τ_{rec} strongly supports the possibility of magnetic recon-

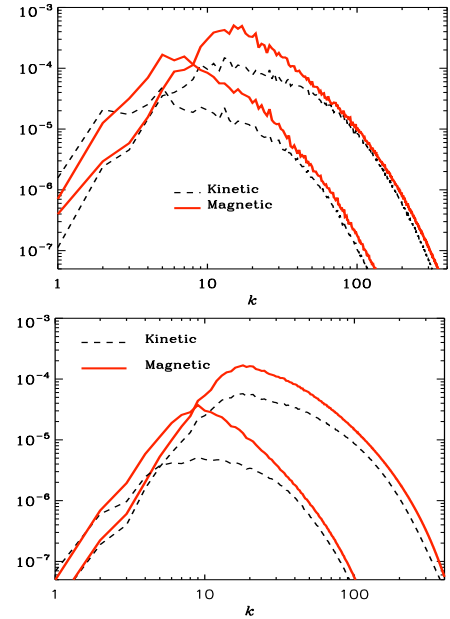


Figure 9. Magnetic and kinetic power spectra plotted at times, $t = 2$ and 12 from the 2D and 3D runs, A2D and A3D, in upper and lower panels respectively.

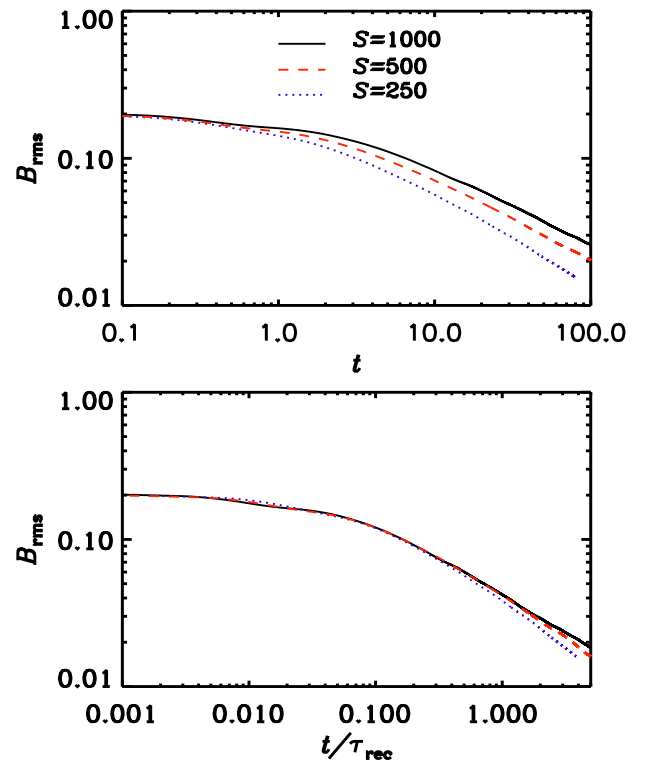


Figure 10. Time evolution of B_{rms} from 2D runs with varying values of S . In the lower panel, the time axis has been normalized by the reconnection timescale τ_{rec} pertaining to each value of S .

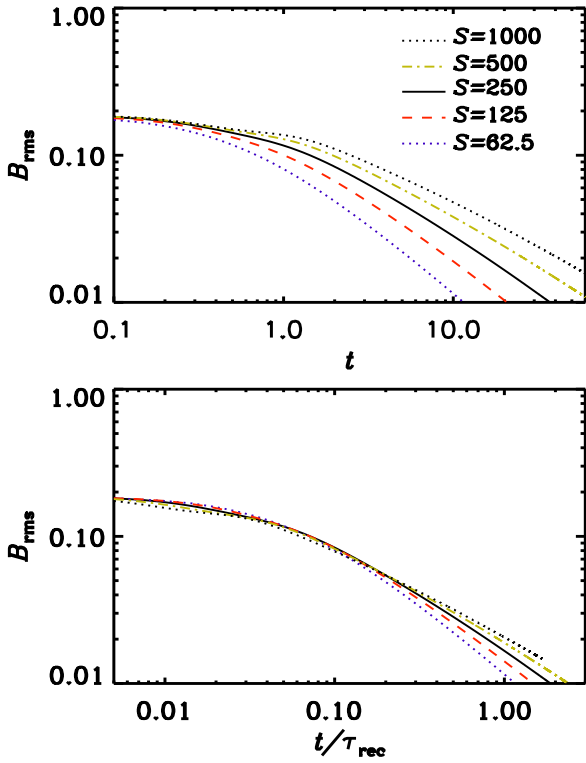


Figure 11. Time evolution of B_{rms} from 3D runs with varying values of S . In the lower panel, the time axis has been normalized by the reconnection timescale τ_{rec} .

nection being the key mechanism responsible for this 3D nonhelical inverse transfer.

3.3 Energy transfer functions

The previous sections have provided both qualitative and quantitative information in support of the notion that magnetic reconnection is the physical mechanism underlying the inverse transfer that we observe in both the 2D and 3D simulations. Additional arguments consistent with this conclusion arise from the analysis of the energy transfer functions, as we discuss in this section.

We calculate spectral transfer functions involving transfer between different scales in the magnetic energy, given by T_{bb} , between magnetic and kinetic energies, given by T_{ub} , and between different scales in the kinetic energy, given by T_{uu} . For the calculation of the transfer functions, we follow the formalism discussed by Grete et al. (2017). The transfer function $T_{xy}(Q, K)$ denotes the transfer of energy from shell Q to shell K , with the subscript referring to the energy reservoir, u for kinetic energy and b for magnetic energy. In other words, $T_{xy}(Q, K) > 0$ denotes a transfer from the reservoir x to y , and $T_{xy}(Q, K) < 0$ denotes transfer from y to x . These functions are antisymmetric when $x = y$, i.e., T_{uu} and T_{bb} .

The transfer functions are given by

$$T_{bb}(Q, K) = - \int B^K \cdot (u \cdot \nabla) B^Q + \frac{1}{2} B^K \cdot B^Q (\nabla \cdot u) dx, \quad (12)$$

$$T_{ub}(Q, K) = \int B^K \cdot \nabla \cdot \left(\frac{B}{\sqrt{\rho}} \otimes w^Q \right) - B^K \cdot B \nabla \cdot \left(\frac{w^Q}{2\sqrt{\rho}} \right) dx, \quad (13)$$

$$T_{uu}(Q, K) = - \int w^K \cdot (u \cdot \nabla) w^Q + \frac{1}{2} w^K \cdot w^Q (\nabla \cdot u) dx, \quad (14)$$

where \otimes denotes tensor product, $w = \sqrt{\rho}u$, and the shell-filtered quantities in real space are given by $\hat{\phi}^K(x) = \int_K \hat{\phi}(k) e^{ik \cdot x} dk$.

We intend to look for signatures of magnetic reconnection in the transfer function plots calculated from our simulations. Energetically, MHD reconnection involves energy transfer from the magnetic to the velocity fields, manifested by the Alfvénic outflows along the length of the current sheet that it generates. There is also, in addition, Ohmic dissipation in the current sheet.

In previous sections, we have mentioned that the merging of magnetic islands facilitated by reconnection results in inverse transfer in a 2D system; these mergers take place in hierarchical fashion, where each generation of mergers produces islands of larger sizes, which then merge to produce larger islands, and so on (Zhou et al. 2019). We conjecture that the 3D system evolves in a similar way, with reconnection merging current filaments, and resulting in an inverse cascade of magnetic energy. If this conjecture is true, then we expect to observe, at any given point in time, significant transfer of magnetic to kinetic energy at a scale corresponding to the dominant island size at that time (the current sheet length scales as the size of the islands).

We suppose that the 3D system evolves in a similar way, with reconnection merging current filaments, and resulting in an inverse cascade of magnetic energy. Given this theoretical understanding, we have the following expectations for the transfer function plots:

(i) In the T_{bb} plot, the scales at which the merging of islands (or current filaments) predominantly takes place (corresponding to k_{corr}) should exhibit inverse transfer, while rest of the (smaller) scales should decay or direct transfer to further smaller scales.

(ii) In the T_{ub} plot, the transfer from magnetic to kinetic energy should stand out at scales comparable to those at which the inverse transfer (i.e., reconnection) is dominant.

(iii) In the T_{uu} plot, there should be a similarity with the T_{bb} plot as the flows accompanying the fields will behave similarly.

Note that the expectations for the behaviour of transfer functions for a system where magnetic reconnection drives the inverse transfer are quite specific, as opposed to a case where a generic turbulence-related process drives the inverse transfer. For example, in a generic turbulence-related process, we do not expect the transfer from the magnetic to the velocity fields to be concentrated around certain scales, but to be spread out over a wide range of scales.

In the upper panel of Fig. 12, the T_{bb} plot from a 2D simulation shows both inverse and direct transfer of energy for certain ranges of scales. Notice that the reflection of the patterns around the diagonal is due to antisymmetry. Next, observe that on the lower side of the diagonal, there is a change in the dominant color of red

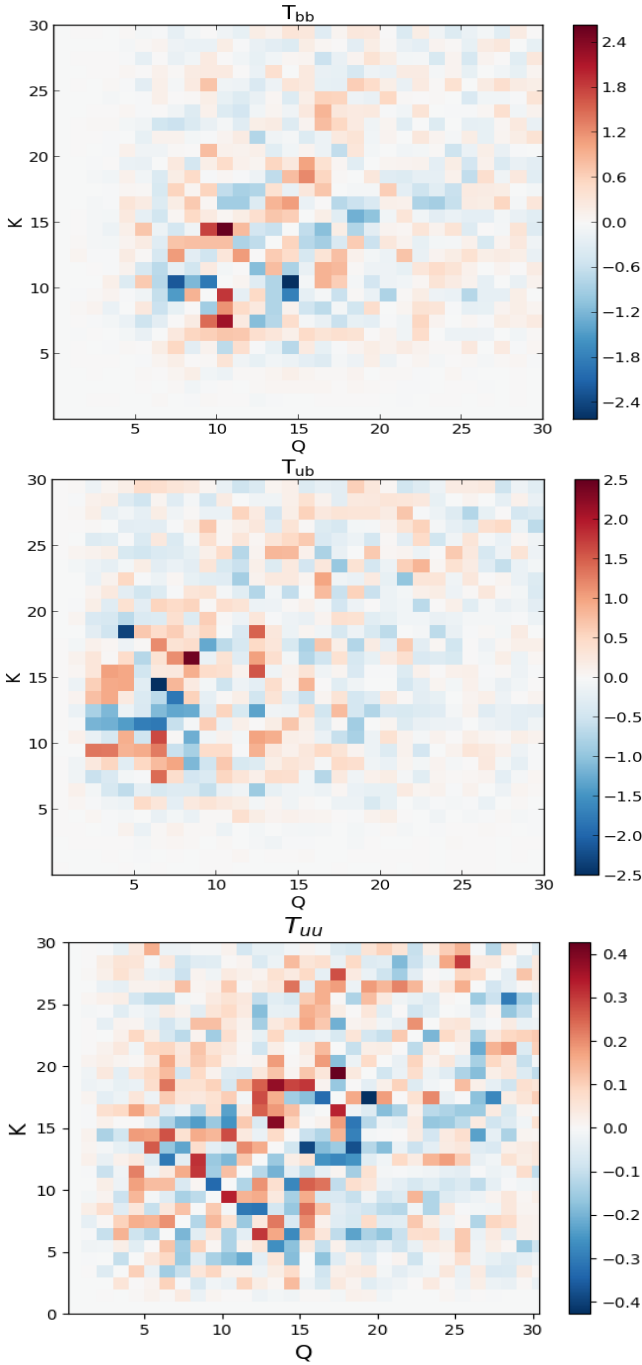


Figure 12. Top, middle and bottom panels show the transfer functions T_{bb} , T_{ub} and T_{uu} , respectively, from the 2D simulation A2D. At this point of time, $t = 10$ in the simulation, $k_p \sim 9$.

in lower wavenumbers to the dominant color of blue in the higher wavenumbers. This means that there is inverse transfer of energy from $Q = 10$ to $K = 6-9$ indicated by the red color, and for $Q > 10$ forward transfer is dominant, as indicated by the blue color.

In the middle panel of Fig. 12, the T_{ub} plot shows that energy transfer from the magnetic field to the velocity field is from $K = 11 - 14$ to $Q \sim 6$, as indicated by the blue patch. Since the blue color refers to negative values, it implies the direction of the

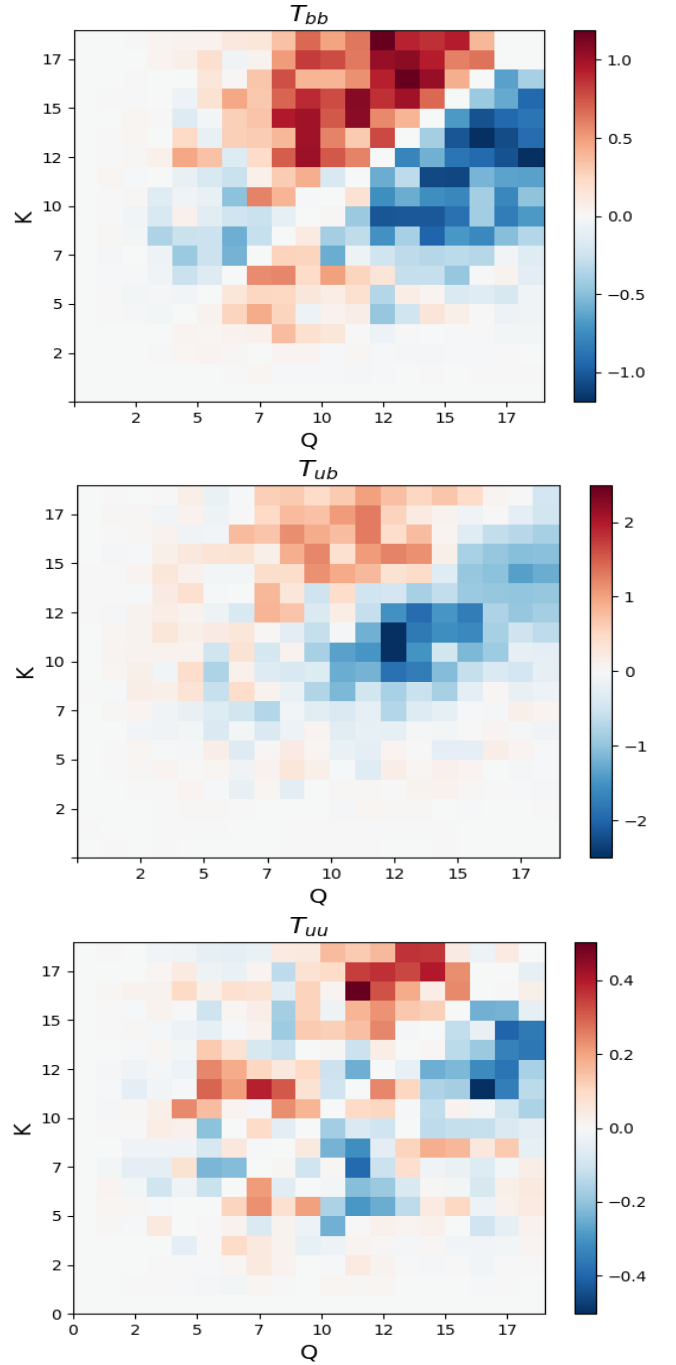


Figure 13. Top, middle and bottom panels show the transfer functions T_{bb} , T_{ub} and T_{uu} , respectively, from the 3D simulation C3D. At this point of time, $t = 20$ in the simulation, $k_p \sim 9$.

transfer to be from K to Q and thus from the magnetic to the kinetic energy reservoirs. This confirms that the transfer is localized to a certain set of scales as expected for a phenomenon (reconnection) dependent process as opposed to a generic turbulence driven process.

The bottom panel of Fig. 12 shows the T_{uu} plot. Below the diagonal line, the darkest red spot at $Q = 10$ and the surrounding small red patch is indicative of minor inverse transfer of energy. This is mainly due to the reasoning that as the magnetic structures

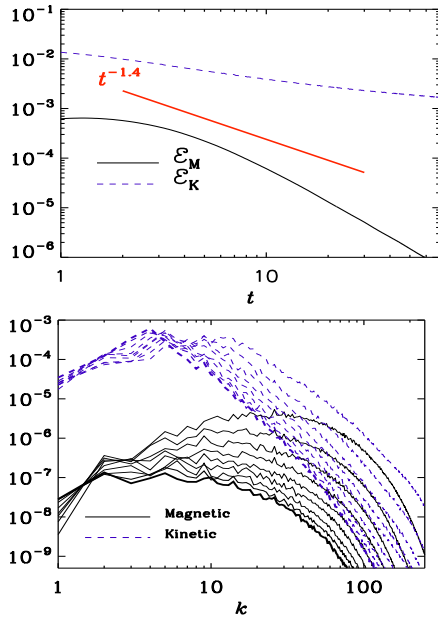


Figure 14. Top panel: Evolution of magnetic energy (solid black) and kinetic energy (dashed blue) in a 2D simulation, F2D, with non-zero initial velocity. Bottom panel: Magnetic and kinetic power spectra from the same simulation, plotted at regular intervals of $\Delta t = 5$, with a thick final curve at $t = 45$.

merge, the underlying flow structures also acquire a larger size. In that sense, the features in T_{uu} plot mimic the T_{bb} plot. Also, given that the flow is energetically subdominant to the field, the T_{uu} transfers are expected to be small.

Similarly, we show transfer function plots for the 3D case in Fig. 13. In the plot of T_{bb} , we find that the pattern changes trend around $Q \sim 10$. The scales larger than the wavenumber $Q \simeq 10$ exhibit inverse transfer (these are the scales where reconnection would be taking place), while $Q \geq 10$ show forward transfer, as expected. In the plot for T_{ub} , the transfer from magnetic to kinetic reservoirs is localized around $Q \sim 12$ and $K \sim 10$, as expected from a reconnection-dependent process dominantly happening at these scales. Again, as in 2D case, the T_{uu} plot here in 3D shows similarity to the T_{bb} plot, with a minor inverse transfer of energy from around $Q = 7$. Note that the energy transfers are mostly local and thus the patterns seen in all the plots are mostly concentrated around the diagonal in both 2D and 3D cases.

The 2D and the 3D transfer function plots tell a similar story — with greater clarity in the 3D case, we think, because turbulence in that limit is unconstrained. The behaviour of the transfer functions is what is expected for a magnetic-reconnection-driven inverse cascade.

3.4 The case when the initial velocity field is non-zero

In all our simulations up until this point, the velocity field was initialized to be zero. The flows that arose in these simulations were generated by the magnetic field, and were shown to be subdominant to it. Magnetic reconnection is typically accompanied by the conversion of magnetic to kinetic energy. These generated flows, thus, are largely Alfvénic in nature. And such flows, where \mathbf{u} and \mathbf{B} are mostly parallel, lead to negligible induction.

However if the velocity field is non-zero (and the system is not magnetically dominated) to begin with, it can lead to a non-trivial

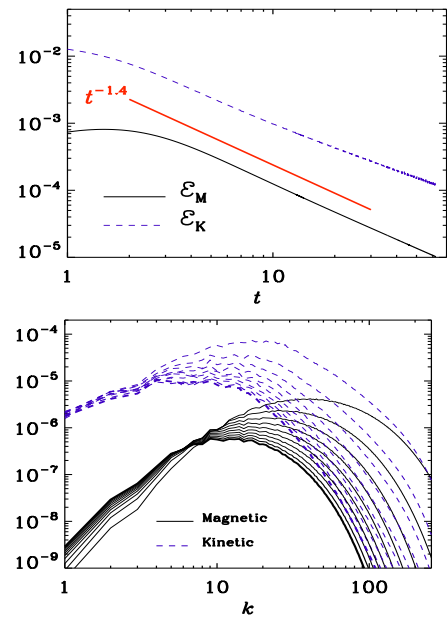


Figure 15. Top panel: Evolution of magnetic energy (solid black) and kinetic energy (dashed blue) in a 3D simulation, F3D, with non-zero initial velocity. Bottom panel: Magnetic and kinetic power spectra $M(k, t)$ plotted at regular intervals of $\Delta t = 5$, with a thick final curve at $t = 50$.

stretching term ($\mathbf{B} \cdot \nabla \mathbf{u}$), resulting in conversion of kinetic to magnetic energy. Then the simple arguments for showing $\lambda_A \ll \lambda_B$ will not hold true anymore. This invites the question that if we consider a non-zero initial velocity field, will we observe energy decay of a different nature, one without an inverse transfer? To clarify this question, we have also performed simulations where the initial velocity field is not only finite, but dominant, which we discuss in this section.

We first examine the 2D case (run F2D). We initialize the flow field in a manner similar to the magnetic field, as specified in section 2.2. While the slope of the magnetic power spectrum is set to k^4 , the kinetic spectrum is set to k^2 (chosen because this is the slope that develops in the runs when the initial velocity field is zero). Also, u_{rms} is initialized to be larger than B_{rms} by a factor of 10. In Fig. 14, we show the evolution curves of the magnetic and kinetic energies, and also their spectra. It is seen that there is no inverse transfer in energy (there is a minor growth at the $k = 1$ which we will address below), and also the temporal scaling of the magnetic energy evolution curve is much steeper than the $\sim t^{-1}$ evolution found in the case of zero initial velocity (Fig. 1).

Next, we show in Fig. 15 the evolution curves of the magnetic and kinetic energies, and their spectra, for the 3D case (run F3D). Here, surprisingly, we do find an inverse transfer. However the magnetic energy (and the kinetic energy) does not evolve as $\sim t^{-1}$ but as $\sim t^{-1.4}$. This numerical scaling of $\sim t^{-1.4}$ is close to the decay law of $\sim t^{-10/7}$, as governed by the Loitsyanky invariant (Davidson 2000) (obtained in the case of hydrodynamic turbulence but not unreasonable to consider here, given the dominance of the kinetic energy).

It is not at once obvious why there is a continued inverse transfer behaviour also when the initial kinetic energy is non-zero in the 3D case. To understand this, we have to consider that there exists a crucial difference between 2D and 3D cases with respect to dynamo action. It is well-known from anti-dynamo theorems (Moffatt 1978; Zeldovich 1957) that there can be no sustained dynamo action in

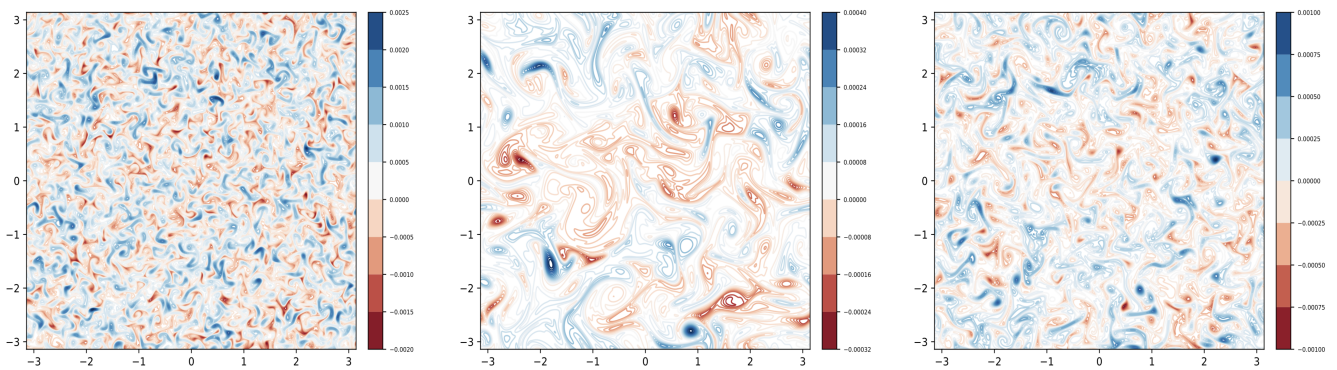


Figure 16. Evolution of the vector potential (A_z) from the 2D simulation, F2D, with non-zero initial velocity shown in contour plots at times $t = 2$, $t = 10$ and $t = 40$ from left to right.

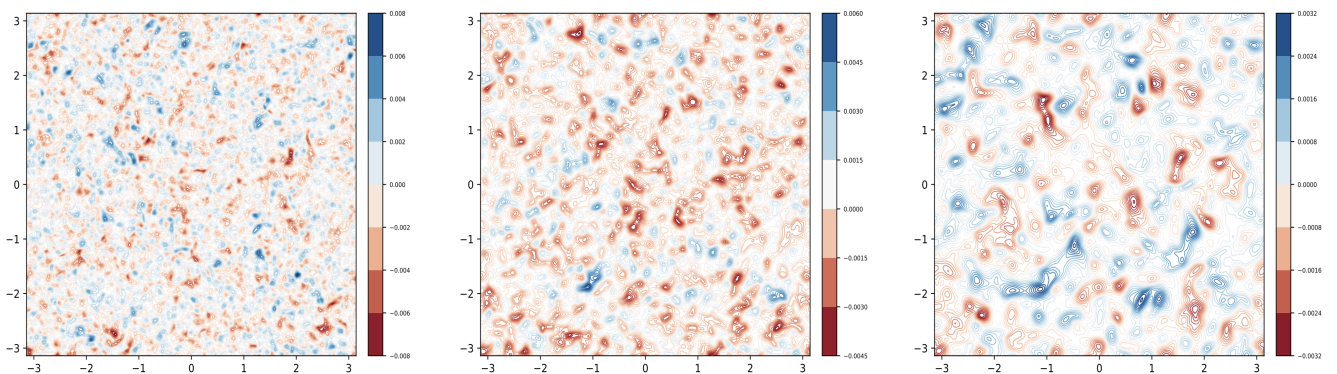


Figure 17. Evolution of a component of the vector potential (A_z) in an arbitrary 2D slice (in $x - y$ plane) from the 3D domain of the 3D simulation, F3D, with non-zero initial velocity shown in contour plots at times $t = 5$, $t = 20$ and $t = 60$ from left to right.

2D. A random velocity field can give rise to anomalous diffusion. In the absence of any sustained dynamo action, such an anomalous diffusion can lead to rapid decay of the field in 2D. In Fig. 16, it can be seen that the system indeed looks turbulent. The stretching of the fields by turbulence can grow the fields in a certain direction while thinning them out in the perpendicular direction. Thus, even though the structures seem to grow in size over time, they are extremely thin and drawn out.

In 3D, besides an anomalous diffusion, these same underlying random motions can also lead to a dynamo, which can mitigate the effect of the anomalous diffusion. The presence of dynamo in our 3D simulations with initial flow can be seen from the top panel of Fig. 15, where the B_{rms} actually increases slightly before it decays. The dynamo effect could explain the difference in the nature of decay of magnetic fields in 2D and 3D, when fields are subdominant to random flows.

In Fig. 17, we find that on a 2D plane from within the 3D domain, the magnetic fields structures are not as drawn out as in the 2D case. They, in fact, retain a more definitive form similar to the earlier cases, as in Figs. 2 and 5. It is not clear if magnetic reconnection has a role to play in the inverse transfer seen in the 3D case. To investigate this further we now study the transfer function plots obtained for the 3D case.

Fig. 18 presents the energy transfer function plots for the run H3D. Even though the spectra in Fig. 15 show the signature of in-

verse transfer, a corresponding distinctive signature in T_{bb} is lacking. The red spots below the diagonal (or equivalently, the blue spots above the diagonal), which indicate inverse transfer, are very few. Here, direct or forward transfer dominates the plot. Also the T_{ub} plot is dominated by red color, indicating that the transfers are from kinetic to magnetic energy, supporting a scenario of dynamo action. Similarly, the T_{uu} plot mostly shows forward transfers as one would expect for a fairly turbulent flow. Thus, overall, the transfer function plots in this case of non-zero initial velocity, fail to uncover any signatures of reconnection-based inverse transfer.

Nonetheless, an interesting feature can be observed in the T_{ub} plot. While most of the energy transfers are from low wavenumbers in the kinetic energy reservoir to the high wavenumbers in the magnetic energy reservoir, there is also energy transfer to smaller wavenumbers. For example, the wavenumber $Q = 10$ contributes significant energy to $K = 7 - 9$. This could be the tail of the small-scale dynamo at low wavenumbers (Haugen et al. 2004; Bhat & Subramanian 2013). Then the question which arises is why is there an inverse transfer in decaying turbulence with dynamo effects. In such a system, the eddies which are supercritical to carry out the dynamo action would pertain to the peak in the kinetic spectrum. It can, then, be seen from the Fig. 15, that due to selective decay, this peak shifts to the lower wavenumbers. As the peak in the kinetic spectrum shifts, it could also shift the scales at which the magnetic energy grows, thus leading to an effect that resembles the inverse

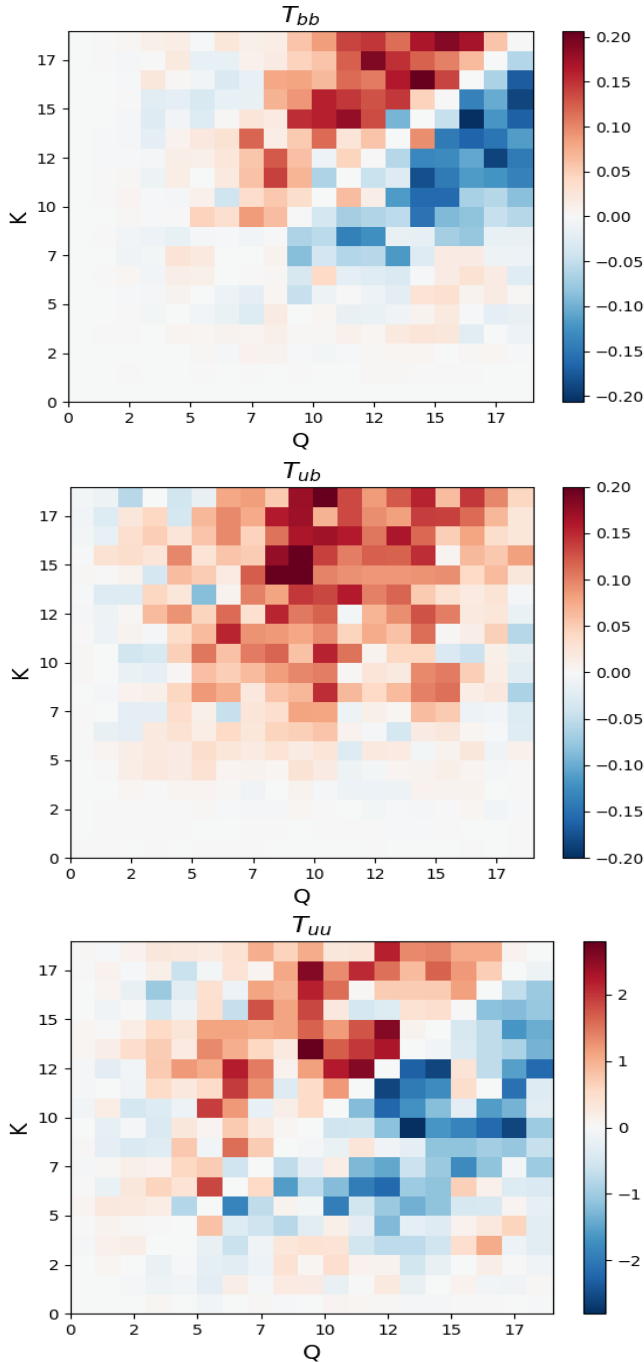


Figure 18. Top, middle and bottom panels show the transfer functions T_{bb} , T_{ub} and T_{uu} , respectively, from the 3D simulation F3D, with non-zero initial velocity. At this point of time, $t = 30$ in the simulation, $k_p \sim 9$.

transfer. A similar effect of flow (which exhibits inverse transfer) dragging the field could be the reason for the growth of magnetic energy at $k = 1$ as seen in Fig. 14 in the 2D simulation, F2D. A more detailed investigation of the case of non-zero initial velocity field in decaying nonhelical MHD turbulence is left to a future paper.

4 DISCUSSION AND CONCLUSIONS

We have investigated the inverse transfer of magnetic energy in the decay of nonhelical MHD turbulence in 2D and 3D simulations. We find that the scaling of magnetic energy with time ($\sim t^{-1}$) and that of power spectrum with wavenumber ($\sim k^{-2}$) is similar between both 2D and 3D cases (when the initial velocity field is zero). This is suggestive of similar mechanisms being responsible, in both cases, for the inverse transfer. In the 2D case, Zhou et al. (2019) have shown that island mergers via magnetic reconnection are key to understanding formation of larger and larger structures that lead to inverse transfer. We find that our simulation results support the idea that magnetic reconnection is responsible for the inverse transfer in 3D nonhelical turbulent systems as well.

Our investigations have yielded two main results via the study of conserved quantities, timescales, and length scales (via transfer function plots). In 2D MHD, the ideal invariants include energy and vector-potential squared. We have provided analytical arguments to show that in a turbulent system, for large Lundquist numbers, vector-potential squared P is better conserved than magnetic energy \mathcal{E}_M (the dominant component of energy in our system) and how, for a decaying system, this can lead to inverse energy transfer. We have calculated the rate of change of the two ideal invariants from the 2D simulation and shown that indeed P is better conserved than \mathcal{E}_M . Further, we found that this was the case even in the 3D simulations, indicating that the dynamics in 3D have 2D-like tendencies. This is our first main result.

Our second main result is that this inverse transfer, both in 2D and in 3D, is due to magnetic reconnection. Indeed, on normalizing the time axis by the magnetic reconnection timescale, we find the evolution curves of the magnetic energy from runs with varying values of Lundquist numbers collapse on top of each other in both 2D and 3D (the collapse being better with larger values of S). Additionally, the transfer function plots show clear signatures of magnetic reconnection driving the inverse transfer. We find from the T_{bb} plots that only those scales either at or above the peak correlation scale, at any given time, exhibit inverse transfer as expected from a physical picture of island (or filament) mergers being dominant at a certain scale. The more clinching evidence arises from the T_{ub} plots, where it is seen that a set of scales compatible with our understanding of the reconnection process in this system stand out in the transfer of magnetic to kinetic energy.

From these results, an emergent characteristic of the magnetically dominated 3D system is its tendency to align with the behaviour observed in 2D. The overarching question is then what element in 3D renders it with 2D-like behaviour? We think the answer lies in the fact that the system is magnetically dominated. The field can provide anisotropy at small-scales i.e. the current sheets can have local guide fields. Magnetic reconnection in 3D, when presided by guide field, leads to familiar 2D results (Onofri et al. 2004). Indeed, in another recent study of inverse energy transfer using the reduced-MHD model (which assumes a strong background magnetic field), Zhou et al. (2020) find mergers between magnetic flux tubes driving inverse transfer.

Returning to the result of k^{-2} slope in the magnetic power spectrum, it has been pointed out that this corresponds to the theoretical expectation for weak turbulence (Brandenburg et al. 2015). However Zhou et al. (2019) find in their 2D simulations that it corresponds to the presence of thin current sheets. In accordance with our findings of 2D-like behaviour in 3D, this explanation of thin current sheets for k^{-2} slope may carry over to 3D as well. Zhou et al. (2020) report a $k^{-1.5}$ slope in their reduced-MHD simula-

tions but unlike the case in the simulations here, they also find kinetic energy is not subdominant to the magnetic energy.

To ascertain whether by making magnetic field subdominant, the inverse transfer in energy ceases to appear, we performed simulations where the initial velocity was set to a large non-zero value. In the 2D simulation, the system becomes turbulent leading to much faster decay of energy, likely due to anomalous diffusion and there is no significant inverse transfer. In contrast, in the 3D case, the energy decay follows a $t^{-1.4}$ scaling, and we do observe a definitive signature of inverse transfer in the evolution of the magnetic spectrum. Furthermore, the evolution of magnetic energy reveals a dynamo effect which possibly counters the anomalous diffusion, leading to a decay rate that is slower than the one seen in the 2D case. On studying the transfer function plots for the 3D simulation, we find that the signature for inverse transfer is surprisingly absent in T_{bb} plot. However, the T_{ub} reveals that there is transfer of energy from the kinetic energy reservoir to magnetic energy to both small and large scales, where the larger portion goes to the small scales. This kinetic energy transfer to larger magnetic scales is a possible signature of the tail of small-scale dynamo action at small wavenumbers. This tail can possibly shift further to lower wavenumbers as the peak in kinetic spectrum shifts due to selective decay, leading to an inverse transfer type effect (as seen in the evolving magnetic spectra).

We have mentioned several astrophysical and cosmological applications to which our results might be relevant in the introduction section. In all of the applications mentioned, the astrophysical systems under consideration consist of highly conducting, large Lundquist number (or magnetic Reynolds number) plasmas. The range of Lundquist numbers explored in this paper is limited by the resolution and thus our simulations are in a regime where Sweet-Parker model for magnetic reconnection is valid. However at higher values of S , the nature of reconnection changes with the onset of the plasmoid instability (Loureiro et al. 2007). Recent research has revealed that the plasmoid instability renders the magnetic reconnection rate independent of S for $S \gtrsim 10^4$, with a reconnection rate of $\sim 0.01 V_A$ (Bhattacharjee et al. 2009; Uzdensky et al. 2010; Loureiro & Uzdensky 2016). This would be the timescale to be considered in the astrophysical systems which can be described with the MHD framework. If, instead, the environment under consideration is weakly collisional, the adequate reconnection rate to consider would be faster, on the order of $0.1V_A$ (e.g., Cassak et al. 2017)

A previous study of this problem had shown that the inverse transfer is weak or altogether absent upon increasing the magnetic Prandtl number Pr_M (Reppin & Banerjee 2017). This is consistent with the understanding that magnetic reconnection at higher Pr_M becomes increasingly inefficient (Park et al. 1984). However, it is not clear if at both higher S and Pr_M this trend will continue, as the ensuing plasmoid instability could potentially change it (Loureiro et al. 2013).

In conclusion, we provide a physical understanding to the puzzling and unexpected 3D nonhelical inverse transfer via analysis of direct numerical simulations of magnetically dominated, decaying MHD turbulence. We argue that magnetic reconnection is the physical mechanism responsible for the emergence of progressively larger structures. Further, we show that the behavior in the 3D system is intriguingly similar to that in 2D, possibly because of local anisotropy in this system. These results could have important consequences for a wider range of astrophysical applications.

ACKNOWLEDGMENTS

We thank K. Subramanian for useful feedback on the paper. PB and NFL acknowledge support from the NSF-DOE Partnership in Basic Plasma Science and Engineering Award No. DE-SC0016215. MZ and NFL acknowledge support from the NSF CAREER Award No. 1654168. This project was completed using funding from the European Research Council (ERC) under the European Unions Horizon 2020 research and innovation programme (grant agreement no. D5S-DLV-786780). The simulations presented in this paper were performed on the MIT-PSFC partition of the Engaging cluster at the MGHPCC facility, funded by DOE Award No. DE-FG02-91-ER54109.

REFERENCES

- Asano K., Terasawa T., 2015, MNRAS, 454, 2242
 Baggaley A. W., Barengi C. F., Sergeev Y. A., 2014, PRE, 89, 013002
 Banerjee R., Jedamzik K., 2004, PRD, 70, 123003
 Batchelor G. K., 1969, PoF, 12
 Beck A. M., Dolag K., Lesch H., Kronberg P. P., 2013, MNRAS, 435, 3575
 Berera A., Linkmann M., 2014, PRE, 90, 041003
 Bhat P., Subramanian K., 2013, MNRAS, 429, 2469
 Bhattacharjee A., Huang Y.-M., Yang H., Rogers B., 2009, PoP, 16, 112102
 Biferale L., Musacchio S., Toschi F., 2012, PRL, 108, 164501
 Biskamp D., 2003, Magnetohydrodynamic Turbulence
 Biskamp D., Welter H., 1989, PoF B, 1, 1964
 Blandford R., Yuan Y., Hoshino M., Sironi L., 2017, SSRv, 207, 291
 Brandenburg A., Kahnashvili T., Tevzadze A. G., 2015, PRL, 114, 075001
 Brandenburg A., Käpylä P. J., 2007, NJP, 9, 305
 Brandenburg A., Subramanian K., 2005, PhR, 417, 1
 Burgers J. M., 1948, in , Vol. 1, Advances in applied mechanics. Elsevier, pp 171–199
 Cassak P. A., Liu Y.-H., Shay M., 2017, JPP, 83, 715830501
 Christensson M., Hindmarsh M., Brandenburg A., 2001, PRE, 64, 056405
 Davidson P. A., 2000, JoT, 1, 6
 Davidson P. A., 2004, Turbulence : an introduction for scientists and engineers. Oxford University Press
 Falkovich G., Sreenivasan K. R., 2006, Phys. Tod., 59, 43
 Frisch U., 1995, Turbulence. The legacy of A. N. Kolmogorov. Cambridge University Press
 Fyfe D., Montgomery D., 1976, JPP, 16, 181
 Gao Y., Xu H., Law C. K., 2015, ApJ, 799, 227
 Grete P., O’Shea B. W., Beckwith K., Schmidt W., Christlieb A., 2017, PoP, 24, 092311
 Haugen N. E., Brandenburg A., Dobler W., 2004, PRE, 70, 016308
 Kadomtsev B. B., Pogutse O. P., 1974, JETP, 38, 283
 Kraichnan R. H., 1967, PoF, 10, 1417
 Loureiro N. F., Schekochihin A. A., Cowley S. C., 2007, PoP, 14, 100703
 Loureiro N. F., Schekochihin A. A., Uzdensky D. A., 2013, PRE, 87, 013102
 Loureiro N. F., Uzdensky D. A., 2016, PPCF, 58, 014021
 Mac Low M.-M., Klessen R. S., Burkert A., Smith M. D., 1998, PRL, 80, 2754
 Moffatt H. K., 1978, Magnetic field generation in electrically conducting fluids. Cambridge University Press
 Nazarenko S., ed. 2011, Wave Turbulence Vol. 825 of Lecture Notes in Physics, Berlin Springer Verlag
 Onofri M., Primavera L., Malara F., Veltri P., 2004, PoP, 11, 4837
 Park W., Monticello D. A., White R. B., 1984, PoF, 27, 137
 Parker E. N., 1957, J. Geophys. Res., 62, 509
 Pouquet A., 1978, JFM, 88, 1
 Pouquet A., Frisch U., Leorat J., 1976, JFM, 77, 321
 Pouquet A., Rosenberg D., Stawarz J. E., Marino R., 2019, Earth and Space Science, 6, 351
 Reppin J., Banerjee R., 2017, PRE, 96, 053105

- Samtaney R., Loureiro N. F., Uzdensky D. A., Schekochihin A. A., Cowley S. C., 2009, PRL, 103, 105004
- Schekochihin A. A., Cowley S. C., Dorland W., Hammett G. W., Howes G. G., Quataert E., Tatsuno T., 2009, ApJS, 182, 310
- Sethi S. K., Subramanian K., 2005, MNRAS, 356, 778
- Skrbek L., Sreenivasan K. R., 2012, PoF, 24, 011301
- Strauss H. R., 1976, PoF, 19, 134
- Subramanian K., 2016, RPP, 79, 076901
- Subramanian K., Shukurov A., Haugen N. E. L., 2006, MNRAS, 366, 1437
- Sur S., 2019, MNRAS, 488, 3439
- Sweet P. A., 1958, in Lehnert B., ed., Electromagnetic Phenomena in Cosmical Physics Vol. 6 of IAU Symposium. p. 123
- Uzdensky D. A., Loureiro N. F., Schekochihin A. A., 2010, PRL, 105, 235002
- Yakhot V., Pelz R., 1987, PoF, 30, 1272
- Zeldovich r. B., 1957, JETP, 4, 460
- Zhou M., Bhat P., Loureiro N. F., Uzdensky D. A., 2019, PRR, 1, 012004
- Zhou M., Loureiro N. F., Uzdensky D. A., 2020, JPP, 86, 535860401
- Zrake J., 2014, ApJL, 794, L26
- Zrake J., 2016, ApJ, 823, 39